Available online at www.sciencedirect.com

SciVerse ScienceDirect

Journal of the European Ceramic Society 32 (2012) 2545–2555

www.elsevier.com/locate/jeurceramsoc

Electrical and thermophysical properties of ZrB_2 and HfB_2 based composites

Manab Mallik [a], Ansu J. Kailath [b], K.K. Ray [a], R. Mitra [a,*]

[a] *Department of Metallurgical and Materials Engineering, Indian Institute of Technology, Kharagpur 721302, West Bengal, India*
[b] *National Metallurgical Laboratory, Jamshedpur, Jharkhand, India*

Received 5 November 2011; received in revised form 28 January 2012; accepted 13 February 2012
Available online 7 March 2012

Abstract

Electrical resistivities, thermal conductivities and thermal expansion coefficients of hot-pressed ZrB_2–SiC, ZrB_2–SiC–Si_3N_4, ZrB_2–ZrC–SiC–Si_3N_4 and HfB_2–SiC composites have been evaluated. Effects of Si_3N_4 and ZrC additions on electrical and thermophysical properties of ZrB_2–SiC composite have been investigated. Further, properties of ZrB_2–SiC and HfB_2–SiC composites have been compared. Electrical resistivities (at 25 °C), thermal conductivities (between 25 and 1300 °C) and thermal expansion coefficients (over 25–1000 °C) have been determined by four-probe method, laser flash method and thermo-mechanical analyzer, respectively. Experimental results have shown reasonable agreement with theoretical predictions. Electrical resistivities of ZrB_2-based composites are lower than that of HfB_2–SiC composite. Thermal conductivity of ZrB_2 increases with addition of SiC, while it decreases on ZrC addition, which is explained considering relative contributions of electrons and phonons to thermal transport. As expected, thermal expansion coefficient of each composite is reduced by SiC additions in 25–200 °C range, while it exceeds theoretical values at higher temperatures.

Keywords: B. Composites; C. Thermal conductivity; C. Thermal expansion; C. Electrical conductivity; D. Borides

1. Introduction

Zirconium diboride (ZrB_2) and hafnium diboride (HfB_2) based composites with reinforcements forming silica on oxidation, such as SiC and Si_3N_4 are considered as candidate ultra-high temperature structural materials for use in sharp leading edges and nose cones of atmospheric re-entry vehicles as well as propulsion systems due to their high melting temperatures, resistance to environmental degradation, and desired thermal properties. It is well established in earlier investigations[1–6] that the presence of SiC and Si_3N_4 particles in the ZrB_2 or HfB_2 based composites not only improves sinterability, but also leads to increase in strength, hardness and toughness compared to that of the monolithic matrix phases, while addition of ZrC is known to improve the ablation resistance of these materials.[6,7] In an earlier study,[6] addition of 5 vol.% Si_3N_4 particles to the ZrB_2–20 vol.% SiC composite has been found to enhance both flexural strength and fracture toughness measured at room temperature.

The materials with high thermal conductivity tend to have impressive thermal shock resistance, as the thermal gradients are minimized by enhanced conduction of heat away from a locally heated zone, which is followed by its radiation away from the surface. The values of room temperature thermal conductivities of ZrB_2 and HfB_2 are about 57.9 $W\,m^{-1}\,K^{-1}$ and 105 $W\,m^{-1}\,K^{-1}$, respectively.[8,9] It is well established that ZrB_2 or HfB_2 based composites having 20–30 vol.% SiC particles as reinforcement tend to have higher thermal conductivity than that of the monolithic material.[10–13] This observation has been attributed to significantly higher thermal conductivity of the SiC phase (reported as 125 $W\,m^{-1}\,K^{-1}$ for sintered SiC and 490 $W\,m^{-1}\,K^{-1}$ for single crystals)[8,10,14] compared to that of the aforementioned matrices. Moreover, it has also been reported that SiC addition (>5 vol.%), increases the thermal conductivity of the ZrB_2–$MoSi_2$–SiC composites.[15]

The thermal shock resistance of a given material is known to depend partially on its coefficient of thermal expansion (CTE), which directly influences the amount of thermal strains introduced in the ceramic components used at elevated temperatures. The CTE reported for ZrB_2 and HfB_2 are 5.9×10^{-6} and $6.3 \times 10^{-6}\,K^{-1}$, respectively,[8] in the temperature range of 27–1027 °C. Addition of SiC with lower CTE

* Corresponding author. Tel.: +91 3222 283292; fax: +91 3222 282280.
E-mail address: rahul@metal.iitkgp.ernet.in (R. Mitra).

0955-2219/$ – see front matter © 2012 Elsevier Ltd. All rights reserved.
doi:10.1016/j.jeurceramsoc.2012.02.013

($\approx 4.3 \times 10^{-6}\ K^{-1}$)[16] than that of either ZrB_2 or HfB_2 is known to reduce the thermal expansion of their composites,[17] which in turn is expected to increase the dimensional stability of these materials. It has been previously reported that the nature of interfacial bond as well as the total interfacial area in the reinforced-matrices have a very strong influence on the CTE of the composites in general.[18,19]

Both ZrB_2 and HfB_2-based composites are attractive because of the excellent electrical conductivities of their matrices, which make these materials amenable to electro-discharge machining for the purpose of near-net shaping. It has been observed that the electrical conductivities of the ZrB_2-based composites depend on the volume fractions of the matrix phase.[12,20] Moreover, the results of earlier studies have confirmed the dependence of thermal conductivities of HfB_2 and ZrB_2 based materials at a given temperature on their electrical conductivities, primarily because the former property involves the contribution of electronic mobility, besides that of phonons.[12,13]

The thermal and electrical properties of both ZrB_2 and HfB_2 based composites with similar compositions but with different matrix grain sizes, reinforcement particle sizes, or methods of processing have been often found to differ from one another. Moreover, the presence of additional phases in different amounts is also expected to have effect on both electrical and thermal properties. In particular, the combined effect of SiC, Si_3N_4 and ZrC additions on electrical and thermal properties of ZrB_2–SiC composites is not well-understood, and hence demands further studies to evaluate the role of different constituent phases. The purpose of this study is to examine the effects of Si_3N_4 and ZrC additions on both electrical and thermal conductivities as well as thermal expansion behavior of ZrB_2–SiC composites, and to compare these properties with those of the HfB_2–SiC composite.

2. Experimental procedure

The powders of ZrB_2, ZrC, SiC and Si_3N_4 were obtained from H.C. Starck Ltd. (H.C. Starck GmbH, Im Schleeke, Goslar, Germany), while the HfB_2 powder was obtained from Johnson Matthey (Johnson Matthey Plc., London, UK). The purity of all the as-received powders was ≥99.5%. Furthermore, the average sizes of ZrB_2, HfB_2, ZrC, SiC and Si_3N_4 powder particles were $3.54 \pm 1.2\ \mu m$, $0.8 \pm 0.6\ \mu m$, 4.75 ± 1.7, $2.1 \pm 0.9\ \mu m$ and $3.3 \pm 1.1\ \mu m$, respectively. The powders having average compositions of ZrB_2–20 vol.% SiC (ZS), ZrB_2–20 vol.% SiC–5 vol.% Si_3N_4 (ZSS), ZrB_2–20 vol.% ZrC–20 vol.% SiC–5 vol.% Si_3N_4 (ZZSS) and HfB_2–20 vol.% SiC (HS), were intimately mixed by milling using balls and vials made of WC–Co composite in a planetary mono-mill (Fritsch GmbH, Idar-Oberstein, Germany), operated at a speed of 250 rpm for 2 h. The powder mixtures were sintered under uniaxial pressure of 30 MPa using graphite dies lined with grafoil inside a resistance heating furnace operated at 2000 °C for 30 min in argon environment, to prepare discs having 42 mm diameter and 4 mm thickness.

The densities of the hot pressed composites were measured using the Archimedes' principle. For microstructural studies, the hot pressed pellets were first sectioned with the help of an Isomet slow speed precision cutting diamond saw (Buehler Ltd., Lake Bluff, IL, USA), and then sequentially polished using diamond coated discs, abrasive SiC papers, and clothes smeared with 1 μm or 0.25 μm diamond lapping paste. The phases present in their microstructures were delineated by X-ray diffraction (XRD) analyses. Furthermore, the microstructures of the hot pressed composites were examined on a field emission scanning electron microscope (FESEM, Model: Zeiss Supra 40, Carl Zeiss NTS GmbH, Oberkochen, Germany) using secondary electron (SE) and backscattered electron (BSE) imaging, while the chemical compositions of the constituent phases were determined simultaneously by using an energy dispersive X-ray (EDX) analyzer. The microstructures of the specimens were also examined with the help of a transmission electron microscope (TEM, Model: JEM 2100, JEOL, Japan) operated at an acceleration voltage of 200 kV, to examine primarily the grain boundaries and particle–matrix interfaces. The images were recorded using both bright and dark field microscopy, while the structures of the constituent phases were examined by selected area diffraction (SAD). For estimating the grain size, average dimensions of ≥100 grains were measured in the images obtained from both SEM and TEM using image analyses.

Samples for electrical resistivity and thermal diffusivity measurements were cut from the hot pressed samples using wire electro-discharge machining (EDM). The electrical resistivities of the specimens with diameter of 20 mm and thickness in the range of 2–4 mm were measured at the ambient temperature using the van der Pauw four-probe method with the help of a high precision resistivity unit (Keithley 2182A nanovoltmeter and 6220 current source). The electrical resistivity (R_s) was calculated from the relation:

$$R_s = \frac{\pi t R}{\ln 2} \quad (1)$$

where t is the thickness and R is the resistance of the specimen. The resistances between the pairs of mutually orthogonal contacts were measured, and the results were found to be similar, confirming isotropic nature of electrical properties in the investigated composites.

The thermal diffusivity of the investigated composites was measured by laser flash method following the procedure discussed in ASTM E1461.[21] In this method, disc shaped specimens with 12.7 mm diameter and 1.0 mm thickness were subjected to high intensity short duration radiant energy pulse using a laser beam. The incident energy absorbed on the front surface of the specimen, leads to increase in the rear-face temperature, which is recorded continuously with the purpose of measuring the time required for it to reach 50% of the maximum value, termed usually as the half time ($t_{1/2}$). The thermal diffusivity (a) is calculated from the relation[21]:

$$a = \frac{0.13879 L^2}{t_{1/2}} \quad (2)$$

where L is the specimen thickness and $t_{1/2}$ is the half time. The specific heat (c) of each investigated composite was calculated from the specific heat data available in the literature[22,23] for each constituent phase, and its corresponding weight fraction

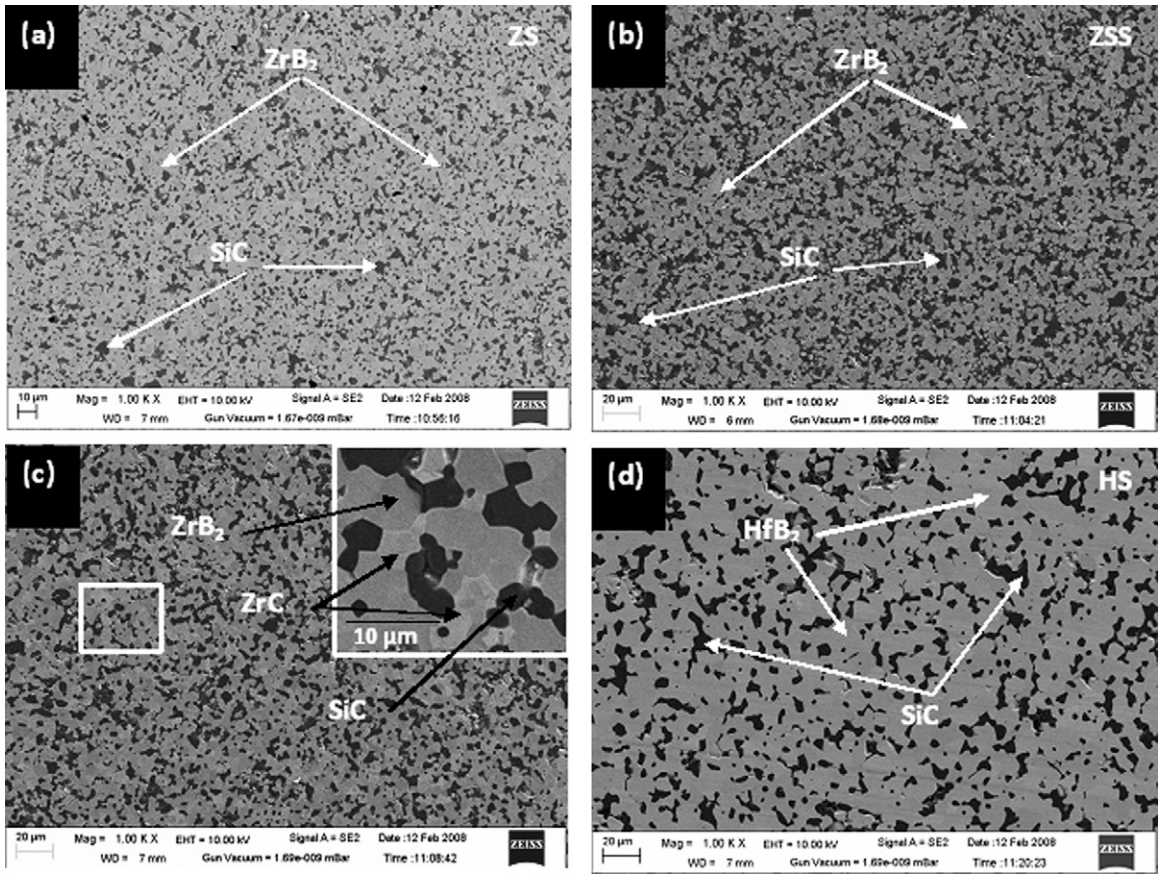

Fig. 1. SEM (SE) images showing the microstructures of: (a) ZS; (b) ZSS; (c) ZZSS and (d) HS composites.

by using the rule of mixtures (ROM). Thereafter, the thermal conductivity (λ) was calculated using the relation[21]:

$$\lambda = ca\rho \tag{3}$$

where ρ is the density of the material measured at 20 °C.

The coefficients of thermal expansion (CTE) of the investigated composites were measured in the temperature range of 200–1000 °C by a thermo-mechanical analyzer (TMA, Model: Diamond TMA, Perkin Elmer, USA). For this purpose, samples with dimensions of 10 mm × 5 mm × 4 mm were sectioned with the help of an Isomet slow speed diamond saw (Buehler Ltd., Lake Bluff, IL, USA) and heated at the rate of 5 °C per minute in argon atmosphere, and the change in dimensions with increase in temperature was continuously recorded. The value of CTE (α) was calculated using the relationship:

$$\alpha = \frac{\Delta L}{L_0 \Delta T} \tag{4}$$

where L_0 is the length of the samples at ambient temperature, $T_0 \sim 20$ °C, ΔL and ΔT are the changes in the length and the temperature, respectively with respect to their initial values.

3. Results and discussion

3.1. Density and microstructure

The bulk densities of ZS, ZSS, ZZSS and HS composites have been found through measurements based on the Archimedes' principle to be 5.50, 5.33, 5.47, and 9.10 g cm^{-3}, respectively. Analysis of these results indicates that the ZrB_2 based and HfB_2 based composites have >98% and ~96% of the theoretical density, respectively.

The SEM (SE) images depicting the microstructures of the hot pressed composites as shown in Fig. 1, confirm more or less uniform dispersion of the constituent phases throughout the matrix. The brighter constituents in these images are ZrB_2 or HfB_2, whereas the darker constituents are usually either SiC or Si_3N_4; the gray level of ZrC is in between that of ZrB_2 and SiC/Si_3N_4 (shown as inset in Fig. 1(c)). The results of microstructural studies carried out on the investigated ZrB_2-based composites have been already discussed in detail elsewhere.[6] Typical bright field TEM images of ZS and ZZSS composites consisting of different phases are shown in Fig. 2(a) and (b), respectively. Furthermore, examination of the microstructure of the ZZSS composite as shown in Fig. 2(b), and supplemented by EDX and SAD analyses at different locations has confirmed that the Si_3N_4 particles with an average size <0.5 μm are present at grain boundaries or interfaces. Based

Table 1
Electrical resistivities and conductivities of the investigated composites.

Materials	Specimen thickness (cm)	Voltage (mV)	Current (mA)	Resistance (μΩ)	Resistivity ($\times 10^{-8}$ Ω m)	Conductivity ($\times 10^{6}$ S/m)
ZS	0.17	0.00133	100	13.3	10.25	9.76
ZSS	0.25	0.00107	100	10.7	12.12	8.25
ZZSS	0.25	0.00185	100	18.5	20.96	4.77
HS	0.40	0.00198	100	19.8	35.90	2.78

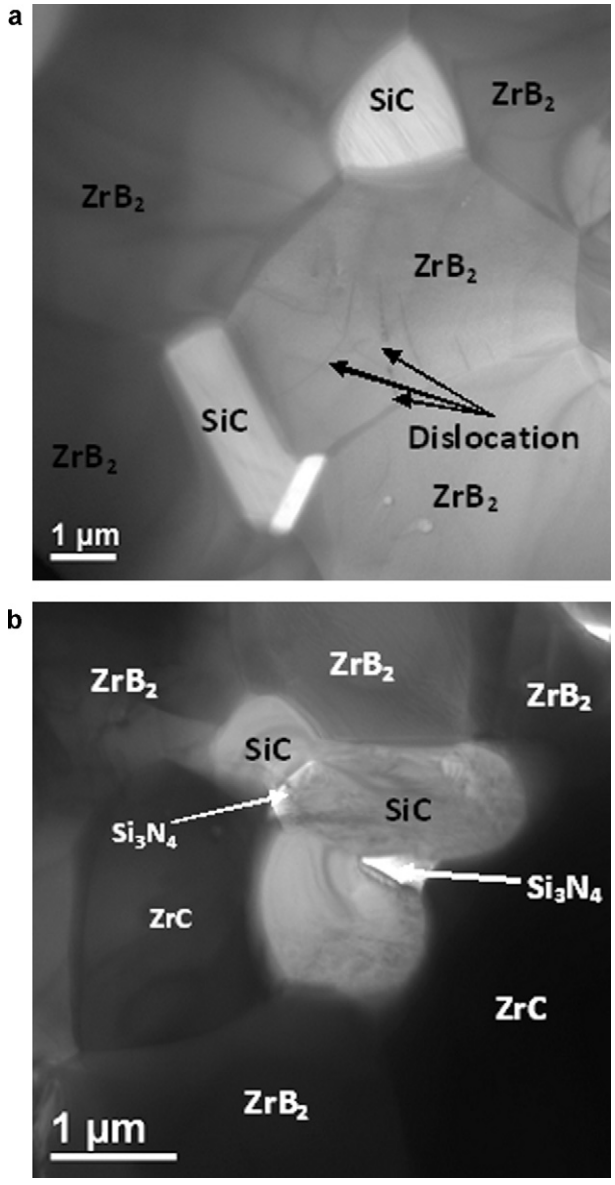

Fig. 2. Bright field TEM images depicting the microstructures of: (a) ZS and (b) ZZSS composites.

on a thorough analysis of both SEM and TEM images of the investigated ZrB_2-based composites, the average sizes of ZrB_2 grains and SiC particles are found to be 5.94 ± 2.25 μm and 5.77 ± 3.49 μm, respectively. In a similar manner, the average sizes of HfB_2 grains and SiC particles in HS have been found to be 6.95 ± 3.04 μm and 5.77 ± 3.49 μm, respectively.

3.2. Electrical resistivity and conductivity

The values of electrical resistivity and conductivity obtained through measurements using the Van der Pauw four-probe method are shown in Table 1. Examination of these results shows that the electrical conductivities of the investigated composites decrease as ZS > ZSS > ZZSS > HS. It is thus obvious that among the ZrB_2-based composites, electrical resistivity increases with both increasing volume fraction of constituent phases having conductivity less than that of ZrB_2, and with increasing area of the constituent interfaces. This observation is consistent with the results of an earlier study by Guo et al.[20] who have reported increase in electrical resistivity with increase in the volume fractions of ZrC and SiC in the ZrB_2 based composites. An increase in the value of electrical resistivity by ≈2.5 times has also been reported by Zhang et al.[13] on addition of 20 vol.% SiC particles to the ZrB_2 matrix. It may be noted that the experimentally measured electrical resistivity of ZS shows excellent agreement with the results (≈10.2 μΩ cm) reported by Tye and Clougherty[10] while it appears to be less than that (≈17.0 μΩ cm) reported by Zhang et al.[13] by as much as ≈70%. The estimated value of electrical resistivity for the ZSS is found to be ≈25% less than that reported for the ZrB_2–20 SiC–4 Si_3N_4 composite by Monteverde et al.[1] The observed variations in the extent of agreement can be considered to originate from the fact that electrical conductivity of the composite is influenced by size, shape, distribution and volume fraction of the reinforcement particles, matrix grain sizes, purity of raw materials as well as the nature of the matrix-reinforcement interfaces.

The results in Table 1 indicate that the HS composite possesses higher resistivity than those of the investigated ZrB_2-based composites, inspite of having the same amount of SiC particulate reinforcement as that of the ZS composite. The possible explanations for such an observation are: (i) the electrical resistivity of the HfB_2 is higher than that of ZrB_2; and (ii) the relative density of the hot pressed HS composite is about 2–3% less than those of the investigated ZrB_2-based composites, as has been mentioned in Section 3.1. Existing literature shows wide variation in the reported values of the electrical resistivity of both ZrB_2 and HfB_2, which are found to vary in the ranges of 6.7–22 μΩ cm[12,24,25] and 6.3–16.6 μΩ cm,[24–26] respectively. The differences between the results in different reports may be attributed to the strong influence of process parameters, relative density of composite, as well as purity and grain size of the constituent phases.

An average value of internal interface electrical resistance has been calculated for the investigated composites using

the following relation suggested by the Brick Layer Model (BLM)[27]:

$$\sigma = \left[\left(\frac{1}{\sigma_{\text{int}}}\right) + \left(\frac{R_{\text{I}}}{d}\right)\right]^{-1} \quad (5)$$

where σ is the electrical conductivity of a typical single phase material (the matrix phase in this study), σ_{int} is the intrinsic electrical conductivity of the matrix phase, R_{I} is the average interfacial electrical resistance, and d is the average matrix grain size. In Eq. (5), the intrinsic electrical conductivity of a given phase is considered to be that of its single crystal. Hence, the value of σ_{int} for ZrB_2 has been considered as $\approx 2.17 \times 10^7$ S/m.[28] The value of σ used in Eq. (5) has been calculated using the effective medium approximation (EMA). In this approach, one or more dispersed phases are present as isolated inclusions surrounded by a medium, that is the matrix with an effective electrical conductivity, σ_{eff}. The value of σ_{eff} for each of the investigated composites is related to the intrinsic conductivities of the constituent phases through the following relation[29]:

$$\sum_{i=1}^{N} \frac{\sigma_{\text{eff}} - \sigma_i}{2\sigma_{\text{eff}} + \sigma_i} f_i = 0 \quad (6)$$

where σ_i and f_i are the conductivity and the volume fraction of the ith phase. For these calculations, the intrinsic electrical resistivity of ZrB_2, HfB_2, SiC, Si_3N_4 and ZrC have been taken as 4.6 μΩ cm,[28] 11 μΩ cm,[8] 5×10^3 μΩ cm,[30] 10^{13} Ω cm[30] and 49 μΩ cm,[31] respectively. The experimentally obtained value of thermal conductivity for each of the investigated composites has been substituted for σ_{eff} in Eq. (6) to determine the value of σ_i ($=\sigma_m$) for the matrix. This is considered as appropriate, as the matrix phase is polycrystalline with resistance contributed by grain boundaries, and therefore its intrinsic conductivity cannot be same as that of single crystal. This value of σ_m has been used as the value of σ in Eq. (5). In this manner, the inter-grain resistance of the matrix phase has been calculated, so as to match the measured value of electrical conductivity. This approach is similar to that followed by Zhang et al.[13]

The values of R_{I} calculated for ZS, ZSS and ZZSS composites have been found to be 1.50×10^{-13} m^2/S, 1.70×10^{-13} m^2/S, and 2.42×10^{-13} m^2/S, respectively. The value of R_{I} calculated for the ZS composite is found to be ≈2 times higher than that reported by Zhang et al.[13] for pure ZrB_2 (0.76×10^{-13} m^2/S), which shows that there is significant increase in the electrical resistance due to the presence of ZrB_2/SiC interfaces in the composite. On further comparison of the aforementioned results pertaining to the investigated ZrB_2-based composites, it is obvious that the value of R_{I} increases with increase in the number of phases possessing lower electrical conductivity than that of the matrix. Considering the σ_{int} of the HfB_2 as 1.35×10^7 S/m,[13] the value of R_{I} has been found as 12.3×10^{-13} m^2/S for the HS composite, which is considerably higher than that obtained for ZS. Thus, it is inferred that higher internal resistance of the HfB_2–SiC interfaces is at least partly responsible for the electrical resistivity of the HS composite being greater than those of the investigated ZrB_2-based composites.

Table 2
Thermal conductivities of the investigated ZrB_2 and HfB_2 based composites. The results of other studies on constituent phases and similar composites are also shown for comparison.

Materials	Temperature (°C)	Thermal conductivity (W/mK)	References
ZS	25	89.53	Present study
ZS	1000	74.79	Present study
ZSS	25	102.74	Present study
ZSS	1000	64.26	Present study
ZZSS	25	81.90	Present study
ZZSS	1000	52.92	Present study
HS	25	141.35	Present study
HS	1000	88.349	Present study
ZrB_2	25	83.8	28
	1000	81.8	8
HfB_2	25	105	32
	1027	60	8
SiC	25	114	33
	1000	35.7	34
Si_3N_4	25	20	35
	1000	26.2	35
ZrC	25	11.5	31
	1500	27.2	36
ZrB_2–20SiC	25	99.2	10
	1000	79.0	10
HfB_2–20SiC	28	128	11
	1000	76	17

3.3. Thermal diffusivity, specific heat and thermal conductivity

3.3.1. Experimental results and theoretical predictions

Plots depicting variations of thermal diffusivity, specific heat and thermal conductivity with temperature for both ZrB_2 and HfB_2 based composites are shown in Fig. 3(a)–(c), respectively. For the purpose of comparison, the results reported by Loehman et al.[17] for pure ZrB_2 and HfB_2 have been included in each of these figures. In addition, the data for both ZrB_2–20 SiC and HfB_2–20 SiC composites as published in earlier reports[11,17] have been also depicted in Fig. 3(c). The thermal conductivities of the investigated composites as shown in Fig. 3(c) have been calculated with the help of Eq. (3) using the experimentally determined values of densities and calculated values of specific heat at different temperatures (Fig. 3(b)). The average values of thermal conductivities of ZS, ZSS, ZZSS and HS composites obtained at the temperatures of 25 °C and 1000 °C are shown in Table 2. The thermal conductivities of monolithic ZrB_2, SiC, Si_3N_4 and HfB_2 used for the theoretical calculations are also shown in this table. Moreover, the results of earlier studies for the composites having similar compositions as those being investigated in this study, have also been included in this table for the purpose of comparison.

The values of thermal conductivity obtained for the investigated materials, as shown in Table 2 are generally found to have moderate to excellent agreement with those found from the published literature. For example, the thermal conductivity of ZS at 25 °C and 1000 °C are found to be reasonably close to the values reported[10,13,17] previously for this composite. On the other

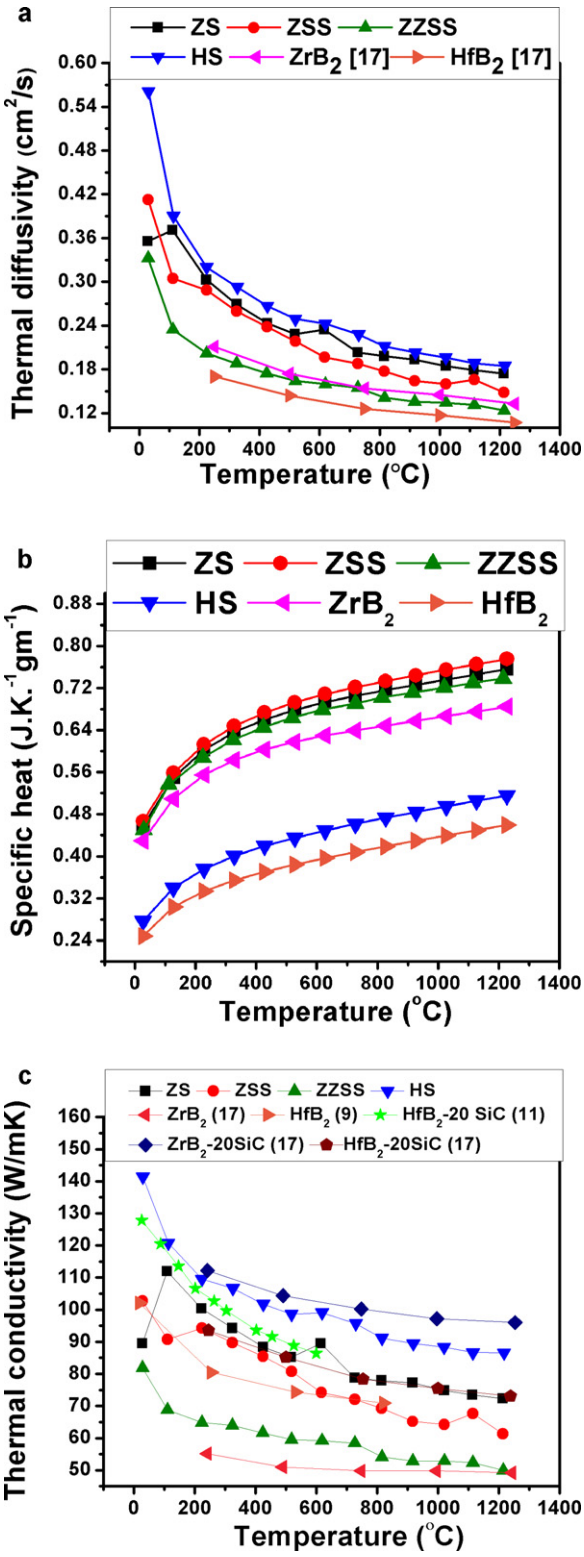

Fig. 3. Plots depicting the variation of: (a) the thermal diffusivity, (b) specific heat and (c) thermal conductivity with temperature for hot pressed ZrB_2 and HfB_2 based composites. The results published in selected earlier reports[9,11,17] are shown for the purpose of comparison.

Table 3
The ratio of electronic component (λ_e) to total thermal conductivity (λ_{exp}) at room temperature (25 °C or 298 K).

Composites	λ_{ph} (W m^{-1} K^{-1})	λ_e (W m^{-1} K^{-1})	λ_e/λ_{exp}
ZS	18.3	71.23	0.8
ZSS	42.5	60.24	0.6
ZZSS	47.1	34.83	0.43
HS	121.02	20.34	0.14

hand, the values determined for the HS are found to be slightly higher than those reported by Zhang et al.[13] for HfB_2–5 vol.% SiC composite within the investigated temperature range, which may be attributed to higher SiC volume fraction in the investigated material. Furthermore, the values obtained for the HS are more than the thermal conductivities reported by Loehman et al.[17] for the composite with identical composition by 9.5 and 14.4% for the tests carried out at 25 °C and 1000 °C, respectively. The differences in this case may be attributed to the finer average sizes of both matrix grains and SiC particles of the composite investigated by Loehman, as compared to those in the HS. Smaller grain size is expected to lead to higher area fraction of interfaces, which in turn, is expected to contribute to greater thermal resistance.[37–39]

The thermal diffusivity at a given temperature has been proposed to be due to the contributions of both electronic transport and phonons in both ZrB_2 and HfB_2 based materials.[12,13] The ratio of electronic component (λ_e) to total thermal conductivity (λ_{exp}) at room temperature (25 °C or 298 K) has been reported by Zhang et al.[13] considering the relation:

$$\frac{\lambda_e}{\lambda_{exp}} = \frac{298L_0}{\rho \cdot \lambda_{exp}} \quad (7)$$

where ρ is the electrical resistivity and L_0 is the Lorenz number whose value has been taken as 2.45×10^{-8} W (Ω K^2)$^{-1}$ by Zhang et al.[13] The ratio of λ_e/λ_{exp}, for the investigated composites has been calculated by the above-mentioned relation, and the estimated values have been included in Table 3. From the results cited in this table, it can be inferred that (i) the ratio of electronic contribution to thermal conductivity decreases as ZS > ZSS > ZZSS > HS; and (ii) among the ZrB_2-based composites, the electronic component of thermal transport decreases with decreasing volume fraction of ZrB_2. Moreover, the thermal conductivity is found to fall more sharply with temperature for all the composites other than ZS, which is suggestive of the greater role of the decrease in the mean free path for phonon scattering in these materials (composites other than ZS). Examination of the results in Table 3 shows that the electronic component is proportional to volume fraction of ZrB_2 phase in the investigated ZrB_2-based composites. Hence, based on the results of electrical conductivity measurements, it is possible to propose that thermal transport is facilitated by electrons in the ZrB_2 phase, and by phonons in the other constituent phases. This observation is also consistent with the value of λ_e/λ_{exp} being reported as $\approx$1.0 for pure ZrB_2 by Zhang et al.[13] Thus, through examination of the results in Table 3, it is appropriate to infer that the contribution of free electron movement is more significant than

that of phonons to thermal transport in case of the investigated ZrB_2-based composites. It may be noted that the electronic contribution of 79% found for the ZS in the present study is close to that reported earlier by Tye and Clougherty[10] for a composite with similar composition but having ZrB_2 grain size of 13 μm, which is more than two times the average size of matrix grains in the investigated composite. This observation suggests that matrix grain size beyond a limiting value probably has negligible effect on electronic or phonon contributions to thermal conductivity.

From the value of λ_e/λ_{exp} obtained for the HS composite as shown in Table 3, it is inferred that the electronic transport is much less relevant for thermal transport than that in the investigated ZrB_2-based composites. This observation is probably due to lower electrical conductivity of the former material, as shown in Table 1. It may be noted that in case of the HfB_2–SiC composites, the value of λ_e/λ_{exp} has been found to decrease from 0.93 to 0.83 on change of SiC volume fraction from 5 to 3%, while in the case of pure HfB_2, this ratio has been found to decrease from 1.0 to 0.92 on decrease in relative density from >98% to ≈92%.[13] Probably, a systematic study needs to be carried out by evaluating thermal and electrical conductivities of the HfB_2-based composite by varying the SiC volume fraction up to 20% for a complete understanding of the role of SiC content in these materials. From the observations reported in the literature,[13] it is inferred that the electronic component of thermal conductivity in the HfB_2-based materials is very sensitive to both relative density and SiC content.

The decrease in both thermal diffusivities and conductivities of the investigated materials with increasing temperature, as shown in Fig. 3(a) and (c), respectively, can be attributed to lower mean free path for electronic transport and phonon scattering with increase in temperature, as has been pointed out by Zimmermann et al.[12] Moreover, the presence of interphase interfaces is expected to have strong influence on phonon scattering, and therefore on the resultant thermal diffusivity of the composites, because of their role in the process of heat conduction by damping of lattice vibrations or phonons.

The average interfacial thermal resistances (R_λ) have been calculated for the investigated ZrB_2-based composites using a modified version of Eq. (5), with σ_{int} and R_I being substituted by λ_{int} and R_λ, respectively, where λ_{int} is the intrinsic thermal conductivity of the matrix phase, and R_λ is the interfacial thermal resistance. Taking $\lambda_{int} \approx 140\,W\,m^{-1}\,K^{-1}$ for ZrB_2[31] and average matrix grain size as ≈5.94 μm, the thermal resistance values of ZS, ZSS and ZZSS composites are found to be $1.7 \times 10^{-8}\,m^2\,(kW)^{-1}$, $0.8 \times 10^{-8}\,m^2\,(kW)^{-1}$ and $3.5 \times 10^{-8}\,m^2\,(kW)^{-1}$, respectively. These values are found to lie well-within the range typically reported in the previous studies[13] on thermal properties of polycrystalline ceramics, that is, 10^{-7}–$10^{-9}\,m^2\,(kW)^{-1}$. Moreover, the values of R_λ observed for the investigated ZrB_2-based composites are 1.3–6 times greater than that reported for the spark plasma sintered ZrB_2 ($R_\lambda \approx 0.6 \times 10^{-8}\,m^2\,(kW)^{-1}$) by Zhang et al.[13] It may be noted that the thermal conductivity value obtained at 25 °C by Zhang et al.[13] for ZrB_2 is greater than that for ZrB_2–20 vol.% SiC composite, which is consistent with lower interfacial or grain boundary thermal resistance in the former material. However, as the thermal conductivity of SiC is greater than that of ZrB_2, thermal transport through the SiC phase is believed to have played a significant role in controlling the thermal conductivity of the investigated composites.

Comparison of the results in Fig. 3(a) and (c) indicates that the thermal diffusivity and conductivity values of both ZS and HS are consistently higher compared to those of monolithic ZrB_2 and HfB_2, respectively at all temperatures, which may be attributed to higher thermal diffusivity of SiC ($0.50\,cm^2/s$ at 20 °C)[40] than those of the matrix phases, and relatively lower interfacial thermal resistances. Moreover, it should be noted that the samples of ZrB_2 and HfB_2 have relative densities of 74% and 68%, respectively. Loehman et al.[17] have reported the thermal diffusivity values of ZrB_2–20 SiC and HfB_2–20 SiC composites at 1000 °C to be $0.17\,cm^2/s$ and $0.20\,cm^2/s$, respectively, which are almost similar to the values (Fig. 3(a)) obtained experimentally in this study. It should also be noted that the thermal diffusivity recorded for the ZZSS has been found to be lower than that of other investigated ZrB_2-based composites due to the presence of a significant amount of ZrC, which has considerably lower thermal diffusivity than that of either ZrB_2 or SiC at any temperature.[35,41] Lower thermal diffusivity of the ZZSS composite compared to that of other ZrB_2 based composites could also be due to higher area fraction of the interfaces contributing to increase in the net resistance to thermal transport in the former material. Examinations of the results depicted in Fig. 3(a) and (c) indicate that compared to the influence of ZrC addition on the thermal diffusivity and conductivity, the presence of Si_3N_4 in the ZSS composite appears to cause much smaller difference with the results observed for ZS. This observation originates probably due to both relatively low volume fraction (5%) of Si_3N_4 and strong interfacial bond in the ZSS composite.

At 25 °C, the thermal diffusivity and specific heat of ZS are found to be less than those of ZSS by ≈16% and ≈2%, respectively, which are responsible for the thermal conductivity of the former material being lower by ≈14.8%. Moreover, the specific heat of SiC is less than that of Si_3N_4 by 5.8% at 25 °C. However, at temperatures >100 °C, the specific heat of SiC is greater than that of Si_3N_4, which in turn is responsible for specific heat of ZS being higher than that of ZSS. In addition, thermal diffusivity of ZS has been found to be greater than that of ZSS at >100 °C, causing the thermal conductivity to be higher as well.

3.4. Coefficient of thermal expansion

3.4.1. Experimental results and theoretical predictions

The plots depicting the variations of linear thermal expansion per unit length ($\Delta L/L_0$) with temperature for ZS, ZSS, ZZSS and HS composites are shown in Fig. 4. The results presented in this figure indicate that for each of the four composites, the thermal expansion per unit length increases with temperature following a linear relationship up to ~1000 °C. For each of the investigated composites subjected to heating from 200 °C to 1000 °C, it can be shown by curve-fitting analysis that the temperature dependence of the measured thermal strains ($\Delta L/L_0$) can be expressed by third-order polynomial expressions having

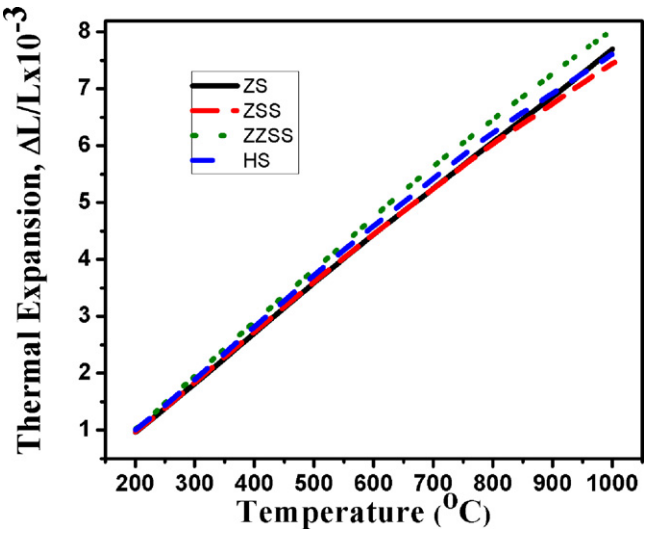

Fig. 4. Plots depicting the variation of thermal expansion per unit length with temperature for ZS, ZSS, ZZSS and HS composites within the temperature range of 200–1000 °C.

R^2 values >0.9999. These expressions are presented as follows:

$$\frac{\Delta L}{L_0}(\mathrm{ZS}) = -0.988 \times 10^{-3} + 9.85 \times 10^{-6} \times T - 1.671 \times 10^{-9} \times T^2 + 4.796 \times 10^{-13} \times T^3 \quad (8)$$

$$\frac{\Delta L}{L_0}(\mathrm{ZSS}) = -0.890 \times 10^{-3} + 9.16 \times 10^{-6} \times T + 9.447 \times 10^{-11} \times T^2 - 9.356 \times 10^{-13} \times T^3 \quad (9)$$

$$\frac{\Delta L}{L_0}(\mathrm{ZZSS}) = -0.900 \times 10^{-3} + 9.4 \times 10^{-6} \times T + 7.094 \times 10^{-10} \times T^2 - 1.184 \times 10^{-12} \times T^3 \quad (10)$$

$$\frac{\Delta L}{L_0}(\mathrm{HS}) = -0.829 \times 10^{-3} + 8.78 \times 10^{-6} \times T + 1.603 \times 10^{-9} \times T^2 - 1.975 \times 10^{-12} \times T^3 \quad (11)$$

The experimentally obtained CTE values of the investigated composites, the values obtained through calculation by considering the rule of mixtures (ROM) and the values of CTE of the individual constituents of the composites as reported in the literature are shown in Table 4. Furthermore, a few results taken from the reports based upon experimental studies on thermal properties of some of the composites with compositions either same as or close to those of the investigated materials are also included in this table for the purpose of comparison.

The trends observed in the CTE of the different composites investigated in this study can be explained qualitatively by consideration of ROM. The results in Table 4 indicate that among the investigated composites, the CTE of ZSS shows the smallest deviation from the value predicted by the ROM for both low and high temperature ranges, which could be due to strong interfacial bonding in this material. As the average CTE of Si_3N_4 is less than that of either ZrB_2 or SiC in the range of 20–1000 °C, its presence is effective in lowering the CTE of the ZSS with respect to those of other investigated materials being tested in the same temperature regime. The results pertaining to ZSS are also consistent with those of an earlier study on the $MoSi_2$–Si_3N_4 composite.[43] Furthermore, the difference between the experimentally determined CTE and the corresponding ROM value is the highest (≈20%) in case of the ZZSS composite, and such a large difference is attributed to the diminished role of SiC in this material due to the presence of ZrC, which has higher CTE than SiC. In an earlier study,[6] the difference between the experimentally determined dynamic Young's modulus and the corresponding value predicted by ROM has been found to be greater for the ZZSS composite than that for either ZS or ZSS. This observation is suggestive of relatively poorer interfacial bond in the ZZSS, which could have contributed to greater deviation of the experimentally obtained CTE with respect to the predicted value.

It is interesting to note that that the differences between the experimentally obtained CTE values and those obtained by the ROM are within ±3–5% within the lower temperature range of 20–200 °C, while such deviations are consistently positive and much greater (approximately 4 times more) in the elevated temperature regime of 20–1000 °C. For example, the CTE value found at 1000 °C for either ZS or ZSS is found to exceed that predicted through the corresponding ROM calculation by ≈14%, while the difference is higher (≈20%) for the ZZSS composite. This observation indicates that the presence of reinforcement phase like SiC or Si_3N_4 with lower CTE as well as a large area fraction of particle–matrix interfaces has significant role in restraining the expansion of the surrounding matrix phase at lower temperatures, but these are not so effective at higher temperatures. It has been proposed by Zimmerman et al.[12] that the SiC particles in the ZrB_2 matrix experience residual stress, which is compressive at lower temperatures due to the differential thermal contraction during cooling from the processing temperature. This stress tends to become tensile on increasing the temperature to or beyond 1000 °C, because the ZrB_2 matrix tends to expand significantly more than the SiC reinforcement. The increased extension of ZrB_2 matrix during heating has been attributed to softening and extension of low-melting matrix grain boundaries or particle–matrix interfacial phases.[17]

Comparison of the CTE values experimentally obtained in this study (as shown in Table 4) for the ZrB_2 based composites with those reported for similar type of materials[1,12,17] shows excellent agreement. On the other hand, the experimentally determined CTE of the HS composite for the temperature range of 20–200 °C (Table 4) appears to be somewhat lower than that (6.10×10^{-6}/°C) reported for a similar temperature

Table 4
Thermal expansion coefficients of the investigated ZrB_2 and HfB_2 based composites, as obtained by experiments and predicted by theoretical calculations using the ROM. The results of other studies on constituent phases and similar composites are shown for comparison.

Materials	Coefficient of thermal expansion (CTE) 10^{-6}/K			
	Temperature range (°C)	Experimental	Predicted by ROM	References
ZS	20–200	5.32	5.56	Present study
	20–1000	7.85	6.74	
ZSS	20–200	5.38	5.36	Present study
	20–1000	7.59	6.56	
ZZSS	20–200	5.61	5.43	Present study
	20–1000	8.20	6.53	
HS	20–200	5.56	5.4	Present study
	20–1000	7.77	6.72	
ZrB_2	25–250	6.68	–	17
	25–1000	7.17	–	
HfB_2	25–250	6.48	–	17
	25–1000	7.15	–	
SiC	20	1.1	–	40
	1000	5.0	–	
Si_3N_4	20–500	2.6	–	42
	20–1000	3.7	–	
ZrC	20–1000	7.01	–	36
ZrB_2–20SiC	25–250	6.21	–	17
	25–1000	6.84	–	
HfB_2–20SiC	25–250	6.10	–	17
	25–1000	6.73	–	
ZrB_2–20SiC–4Si_3N_4	25–800	7.00	–	1
	25–1000	7.48	–	

range by Loehman[17] but shows closer agreement with the value ($\sim 5.4 \times 10^{-6}$/°C) reported by Gasch et al.[44]

3.4.2. Comparison of results with theoretical predictions for two phase materials

Levin[45], Rosen and Hashin[46] and Schapery[47] have independently shown that the linear thermal expansion coefficient of an isotropic two phase composite can be written in its exact form as[27]:

$$(\alpha_{\text{eff}})_u = f_1\alpha_1 + f_2\alpha_2 + \frac{\alpha_1 - \alpha_2}{(1/K_1) - (1/K_2)}\left[\frac{1}{K_{\text{eff}}} - \frac{f_1}{K_1} - \frac{f_2}{K_2}\right] \quad (12)$$

Considering that $K_l \le K_{\text{eff}} \le K_u$, the upper and lower bounds of K can be obtained from the Hashin–Shtrikman bounds.[48] Under such a situation, Eq. (12) can be further modified to calculate both upper and lower bounds of α in the following manner:

$$(\alpha_{\text{eff}})_u = \alpha_1 - f_2(\alpha_1 - \alpha_2)\frac{K_2(3K_1 + 4G_1)}{K_1(3K_2 + 4G_1) + 4f_2G_1(K_2 - K_1)} \quad (13)$$

$$(\alpha_{\text{eff}})_l = \alpha_2 - f_1(\alpha_2 - \alpha_1)\frac{K_1(3K_2 + 4G_2)}{K_2(3K_1 + 4G_2) + 4f_1G_2(K_1 - K_2)} \quad (14)$$

where $(\alpha_{\text{eff}})_u$ and $(\alpha_{\text{eff}})_l$ are the upper bound and lower bounds, respectively, of CTE of the given composite, whereas α, K, G and f are the CTE, bulk modulus, shear modulus and volume fraction, respectively. In these expressions, the subscripts 1 and 2 represent matrix and reinforcement phases, respectively. The values of K and G for ZrB_2, HfB_2 and SiC used for the calculations have been collected from the literature.[40,49]

The Kerner's model[50,51] assumes that the reinforcement is spherical, and is wetted by a uniform layer of matrix. Thus, the composite is stated to be made of volume elements having a spherical reinforcement particle surrounded by a shell of matrix. Using this model, the CTE is found from the relation[50]:

$$\alpha_c = \bar{\alpha} - f_2(1 - f_2)(\alpha_2 - \alpha_1)\frac{K_2 - K_1}{(1 - f_2)K_1 + f_2K_2 + ((3K_1K_2)/(4G_1))} \quad (15)$$

where α is the ROM value given by $\bar{\alpha} = (1 - f_2)\alpha_1 + f_2\alpha_2$, while the subscript, c stands for the composite. The upper and lower bounds of CTE of ZS and HS composites calculated on the basis of the Hashin–Shtrikman relations, as well as theoretical predictions by the Kerner's model and ROM are shown as bar

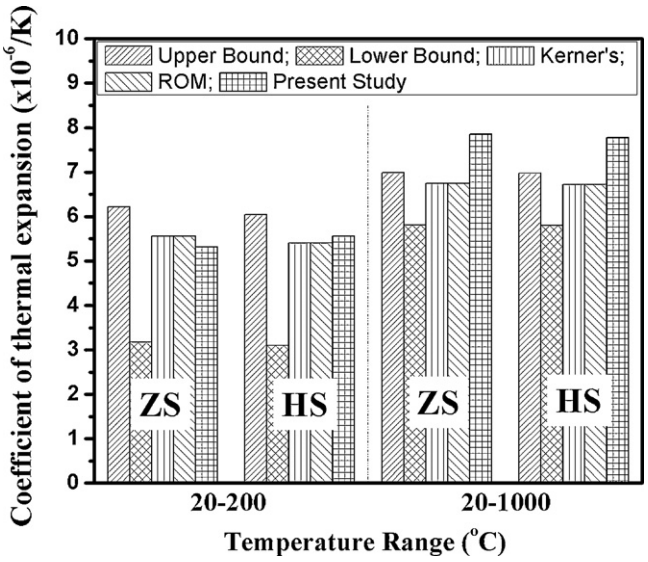

Fig. 5. Bar charts depicting the experimentally obtained CTE of ZS and HS composites in the temperature ranges of 25–200 °C and 25–1000 °C along with results of theoretical predictions.

charts in Fig. 5 along with the experimentally obtained values. A careful comparison of the results in this figure shows that the experimentally obtained CTE values of both ZS and HS in the temperature range of 20–200 °C are remarkably close to both the corresponding values obtained using either ROM or Kerner's model, and are slightly less than the upper limit predicted by the Hashin–Shtrikman relation. On the other hand, the experimental CTE values of both these composites for the temperature range of 20–1000 °C appear to be ≈10% higher than the corresponding upper bound predicted by the Hashin–Shtrikman relation, while the differences with the predictions of ROM and Kerner's model are still greater (13.5–14%).

4. Conclusions

Electrical and thermal conductivities as well as thermal expansion coefficients of ZrB_2–20 vol.% SiC (ZS), ZrB_2–20 vol.% SiC–5 vol.% Si_3N_4 (ZSS), ZrB_2–20 vol.% ZrC–20 vol.% SiC–5 vol.% Si_3N_4 (ZZSS) and HfB_2–20 vol.% SiC (HS) composites have been investigated. The following conclusions may be drawn from the present study:

(i) The electrical resistivity values of the investigated ZrB_2-based composites appear to increase with decreasing ZrB_2 content, and these values have been found to be less than that of the HS composite. The average interfacial resistances between the constituents of the ZrB_2-based composites are found to increase with addition of phases having lower electrical conductivity.

(ii) Addition of 20 vol.% SiC to either ZrB_2 or HfB_2 matrix composites leads to significant increase in their thermal conductivities with respect to those of their monolithic matrices. Presence of 5 vol.% Si_3N_4 in ZSS is found to marginally lower the thermal conductivity. However, addition of 20 vol.% ZrC at the expense of ZrB_2 can be considered responsible for relatively lower thermal conductivity of the ZZSS composite.

(iii) The contribution of electronic transport to thermal conductivity exceeds that of phonons for both ZS and ZSS composites, while it is lower than that of ZZSS and HS composites. The thermal conductivities of these composites are found to decrease with increase in temperature due to lower mean free path for electronic transport and phonon scattering at higher temperatures.

(iv) The variation of linear thermal expansion per unit length with temperature can be best described using third degree polynomial relations. Thermal expansion of each investigated composite is found to be restrained by the presence of SiC in the temperature range of 20–200 °C, in tune with theoretical predictions, while the presence of ZrC in ZZSS is found to increase its CTE. On the other hand, the CTE values of the investigated composites have been found to be higher than the corresponding theoretical predictions at the temperature range of 20–1000 °C, which could be explained due to weakening of both particle–matrix interfaces and matrix grain boundaries with increasing temperature.

Acknowledgments

The financial supports from Defence Research and Development Organization and Central Scientific and Industrial Research, New Delhi are gratefully acknowledged. The authors also express their sincere gratitude to technical personnel at the Central Research Facility, Indian Institute of Technology, Kharagpur, West Bengal.

References

1. Monteverde F, Guicciardi S, Bellosi A. Advances in microstructure and mechanical properties of zirconium diboride based ceramics. *Mater Sci Eng A* 2003;**346**:310–9.
2. Chamberlain AL, Fahrenholtz WG, Hilmas GE, Ellerby DT. High strength ZrB_2 based ceramics. *J Am Ceram Soc* 2004;**87**(6):1170–2.
3. Gasch M, Ellerby D, Irby E, Beckman S, Gusman M, Johnson S. Processing, properties and arc jet oxidation of hafnium diboride/silicon carbide ultra high temperature ceramics. *J Mater Sci* 2004;**39**(19):5925–37.
4. Monteverde F, Bellosi A. The resistance to oxidation of an HfB_2–SiC composite. *J Eur Ceram Soc* 2005;**25**:1025–31.
5. Monteverde F, Melandri C, Guicciard S. Microstructure and mechanical properties of an HfB_2 + 30 vol.% SiC composite consolidated by spark plasma sintering. *Mater Chem Phys* 2006;**100**:513–9.
6. Mitra R, Upender S, Mallik M, Chakraborty S, Ray KK. Mechanical, thermal, and oxidation behaviour of zirconium diboride based ultra-high temperature ceramic composites. *Key Eng Mater* 2009;**395**:55–68.
7. Bull J, White MJ, Kaufman L. Ablation resistant zirconium and hafnium ceramics, US Patent No. 5,750,450; 1998.
8. Cutler RA. In: Schneider SJ, editor. *Engineering properties of borides. Ceramics and glasses, engineered materials handbook*, vol. 4. Materials Park, OH: ASM International; 1992. p. 787–803.
9. Opeka MM, Talmy IG, Wuchina EJ, Zaykoski JA, Causey SJ. Mechanical, thermal and oxidation properties of refractory hafnium and zirconium compounds. *J Eur Ceram Soc* 1999;**19**:2405–14.
10. Tye RP, Clougherty EV. The thermal and electrical conductivities of some electrically conducting compounds. In: *Proceedings of the fifth symposium on thermophysical properties*. 1970. p. 396–401.

11. Gasch M, Johnson S, Marschall J. Thermal conductivity characterization of hafnium diboride-based ultra-high temperature ceramics. *J Am Ceram Soc* 2008;**91**(5):1423–32.
12. Zimmermann JW, Hilmas GE, Fahrenholtz WG, Dinwiddie RB, Porter WD, Wang H. Thermophysical properties of ZrB_2 and ZrB_2–SiC ceramics. *J Am Ceram Soc* 2008;**91**(5):1405–11.
13. Zhang L, Pejakovicǐ DA, Marschall J, Gasch M. Thermal and electrical transport properties of spark plasma-sintered HfB_2 and ZrB_2 ceramics. *J Am Ceram Soc* 2011;**94**(8):2562–70.
14. Lipowitz J, Rabe JA, Zangvil A, Xu Y. Structure and properties of Syralamic^{TM} silicon carbide fiber—a pollycrystalline, stoichiometric β-SiC compostions. *Ceram Eng Sci Proc* 1997;**18**(3):147.
15. Guo S, Kagawa Y, Nishimura T, Tanaka H. Thermal and electrical properties of hot-pressed ZrB_2–$MoSi_2$–SiC composites. *J Am Ceram Soc* 2007;**90**(7):2255–8.
16. Li Z, Bradt RC. Thermal expansion of the hexagonal (6H) polytype of silicon carbide. *J Am Ceram Soc* 1986;**69**(12):863–6.
17. Loehman R, Corral E, Dumm H-P, Kotula P, Tandon R. Ultra-high temperature ceramics for hypersonic vehicle applications. Sandia Report, SAND2006-2925, Albuquerque, NM; June 2006.
18. Xu ZR, Chawla KK, Mitra R, Fine ME. Effect of particle size on the thermal expansion of TiC/Al XD^{TM} composites. *Scr Metall Mater* 1994;**31**(11):1525–30.
19. Park C-S, Kim C-H, Kim M-H, Lee C. The effect of particle size and volume fraction of the reinforced phases on the linear thermal expansion in the Al–Si–SiCp system. *Mater Chem Phys* 2004;**88**:46–52.
20. Guo SQ, Kagawa Y, Nishimura T, Chung D, Yang J-M. Mechanical and physical behavior of spark plasma sintered ZrC–ZrB_2–SiC multiphase composites. *J Eur Ceram Soc* 2008;**28**:1279–85.
21. ASTM E1461-01, Standard test method for thermal diffusivity of solids by the flash method. http://www.astm.org/DATABASE.CART/HISTORICAL/E1461-01.htm; July 21, 2008.
22. Chase Jr MW. NIST-JANAF thermochemical tables. *J Phys Chem Ref Data, Monograph 9*, 4th ed. Woodbury, NY: American Institute for Physics; 1998.
23. Barin I. *Thermochemical data of pure substance, vols. 1–2*. Weinheim, Germany: VCH; 1989.
24. Juretschke HJ, Steinitz R. Hall effect and electrical conductivity of transition-metal diborides. *J Phys Chem Sol* 1958;**4**(1–2):118–27.
25. L'vov SN, Nemchenko VF. Application of one-band concepts to the diborides of group IV transition metals. *Russ Phys J* 1968;**11**(1):36–8.
26. Samsonov GVB, Kovenskaya A, Serebryakova TI. Some physical characteristics of the diborides of transition metals of groups IV and V. *Russ Phys J* 1971;**14**(1):11–4.
27. Ziegler G, Heinrich J, Wotting G. Review of relationships between processing, microstructure and properties of dense and reaction-bonded silicon nitride. *J Mater Sci* 1987;**22**:3041–86.
28. Kinoshita H, Otani S, Kamiyama S, Amano H, Akasaki I, Suda J, et al. Zirconium diboride (0 0 0 1) as an electrically conductive lattice-matched substrate for gallium nitride. *Jpn J Appl Phys* 2001;**40**(12A):L1280–2.
29. Grimvall G. *Thermophysical properties of materials*. North-Holland: Elsevier; 1999. p. 286–300.
30. Nakabayashi M, Fujimoto T, Sawamura M, Ohtani N. Silicon carbide single crystal, silicon carbide single crystal wafer, and method of production of same, US Patent No. 7,794,842; 2006.
31. Williams WS. Transition metal carbides, and borides for electronic applications. *JOM* 1997;**49**(3):38–42.
32. Lawson JW, Daw MS, Bauschlicher Jr CW. Lattice thermal conductivity of ultra high temperature ceramics ZrB_2 and HfB_2 from atomistic simulations. *J App Phys* 2011;**110**:1–4.
33. Goldberg Y, Levinshtein ME, Rumyantsev SL. Silicon carbide (SiC). In: Levinshtein ME, Rumyantsev SL, Shur MS, editors. *Properties of advanced semiconductor materials GaN, AlN, SiC, BN, SiC, SiGe*. New York: John Wiley & Sons Inc.; 2001. p. 93–148.
34. Nilsson O, Mehling H, Horn R, Fricke J, Hofmann R, Muller SG, et al. Determination of the thermal diffusivity and conductivity of monocrystalline silicon carbide (300–2300 K). *High Temp High Press* 1997;**29**:73–9.
35. Hirano T, Izaki K, Niihara K. Microstructure and thermal conductivity of Si_3N_4/SiC nanocomposites fabricated from amorphous Si–C–N precursor powders. *Nanostruct Mater* 1995;**5**(7/8):809–18.
36. Samsonov GV, Vinitskii IM. *Handbook of refractory compounds*. New York: IFI/PLENUM; 1980.
37. Smith DS, Fayette S, Grandjean S, Martin C. Thermal resistance of grain boundaries in alumina ceramics and refractories. *J Am Ceram Soc* 2003;**86**(1):105–11.
38. Fayette S, Smith DS, Smith A, Martin C. Influence of grain size on the thermal conductivity of tin oxide ceramics. *J Eur Ceram Soc* 2000;**20**: 297–302.
39. Yang H-S, Bai G-R, Thompson LJ, Eastman JA. Interfacial thermal resistance in nanocrystalline yttria stabilized zirconia. *Acta Mater* 2002;**50**:2309–17.
40. Munro RG. Material properties of a sintered alpha-SiC. *J Phys Chem Ref Data* 1997;**26**:1195–203.
41. Cape JA, Lehman GW, Nakata MM. Transient thermal diffusivity technique for refractory solids. *J Appl Phys* 1963;**34**(12):3550–5.
42. Munz D, Fett T. *Ceramics: mechanical properties, failure behaviour, materials selection*. New York: Springer; 2001. pp. 10–17.
43. Hsieh T, Choe H, Laverinia EJ, Wolfenstine J. The effect of Si_3N_4 on the thermal expansion behavior of $MoSi_2$. *Mater Lett* 1997;**30**:407–10.
44. Gasch MJ, Ellerby DT, Johnson SM. In: Bansal NP, editor. *Ultra-high temperature ceramic composites*. *Handbook of ceramic composites*. Boston: Kluwer Academic Publishers; 2005. p. 197–224.
45. Levin VM. Thermal expansion coefficients of heterogeneous materials. *Mekhanika Tverdogo Tela* 1967;**2**(1):88–94 [English translation: Mech Solids 2:58–61].
46. Rosen BW, Hashin ZV. Effective thermal expansion coefficients and specific heats of composite materials. *Int J Eng Sci* 1970;**8**:157–73.
47. Schapery RA. Thermal expansion coefficients of composite materials based on energy principles. *J Compos Mater* 1968;**2**:380–404.
48. Hashin Z, Shtrikman SA. Variational approach to the theory of the elastic behavior of multiphase materials. *J Mech Phys Solids* 1963;**11**:127–40.
49. Wiley DE, Manning WR, Hunter OJR. Elastic properties of polycrystalline TiB_2, ZrB_2 and HfB_2 from room temperature 1300 K. *Less Common Met* 1969;**18**(2):149–57.
50. Kerner EH. The elastic and thermo-elastic properties of composite media. *Proc Phys Soc* 1956;**B69**:808–13.
51. Elomari S, Skibo MD, Sundarrajan A, Richards H. Thermal expansion behavior of particulate metal-matrix composites. *Compos Sci Technol* 1998;**58**:369–76.